Gaussian packet prestack depth migration.
Part 2: Optimized Gaussian packets

Václav Bucha

Department of Geophysics, Faculty of Mathematics and Physics, Charles University, Ke Karlovu 3, 121 16 Praha 2, Czech Republic, E-mail: bucha@seis.karlov.mff.cuni.cz

Summary

The algorithm of the Gaussian packet prestack depth migration consists of four basic steps: (a) preparation of a velocity model sufficiently smooth for ray tracing and for application of Gaussian beams and packets, (b) optimization of the shape of Gaussian packets including smoothing, (c) decomposition of the recorded wave field into optimized Gaussian packets, (d) back-propagation of the wave field using Gaussian packets and application of the imaging functional. Žáček (2005) presented a numerical example of applying this Gaussian packet migration to the 2-D acoustic Marmousi model and dataset, but he did not apply the optimization and used the uniform Gaussian packets. We present the application of smoothly optimized Gaussian packets to the Gaussian packet prestack depth migration.

Keywords

Gaussian packets, Gaussian beams, prestack depth migration, common-shot gather, Gabor transform, heterogeneous media.

1. Introduction

The algorithm of the Gaussian packet prestack depth migration described by Žáček (2005) consists of four basic steps:

a) preparation of a velocity model sufficiently smooth for ray tracing and for application of Gaussian beams and packets (Klimeš, 2000; Žáček, 2002),
b) optimization of the shape of Gaussian packets including smoothing (Žáček, 2006a),
c) decomposition of the recorded wave field into optimized Gaussian packets (Žáček, 2005, 2006b),
d) back-propagation of the wave field using Gaussian packets and application of the imaging functional (Žáček, 2005).

Žáček (2005) also presented a numerical example of applying this Gaussian packet migration to the 2-D acoustic *Marmousi model and dataset* (Versteeg & Grau, 1991). He did not apply the optimization and used the uniform Gaussian packets. The results of the migration failed in reconstructing the bottom part of the Marmousi model. Three possible causes of these results were mentioned by Žáček (2005):

a) the use of non–optimized *uniform* Gaussian packets,
b) oversimplified stacking procedure,
c) considerably smoothed velocity models.

The theory of the Gaussian packet migration algorithm is described in the papers cited above. We concentrate here on solving especially computation problems of the Marmousi model numerical example. We present the application of *optimized* (non-uniform) Gaussian packets to the Gaussian packet prestack depth migration.

In: Seismic Waves in Complex 3-D Structures, Report 18 (Department of Geophysics, Charles University, Prague, 2008), pp. 129–138

Updated software (Fortran 77 source codes, data files, history files, descriptions) is included in package DATA (Bucha & Bulant, 2008).

2. Smoothed Marmousi model

We tested the Gaussian packet migration on the Marmousi model and dataset (Versteeg & Grau, 1991). Figure 1 shows distribution of slowness in the Marmousi model, which has been used for calculating the seismograms by finite differences. This model is obviously not suitable for ray tracing. The rays for the Gaussian packet migration has been traced in the velocity model obtained by smoothing the Marmousi model.

The first difference between our computations and those of Žáček (2005) is slightly different velocity model (see Figure 2). The velocity model was prepared by Klimeš (2000) so as to be suitable for ray tracing and for Gaussian-packet migrations. We remind that the standard halfwidths of Gaussian beams indicate that this velocity model is at the edge of applicability of Gaussian beams and Gaussian packets at the considered frequencies which are too low for the application of high-frequency asymptotic methods. Note that the initial conditions for the Gaussian beams should not be constant along the model surface and should be carefully optimized. Without the optimization, we cannot be sure whether the smoothed model is sufficiently smooth or must be smoothed more (for details see Klimeš, 2000).

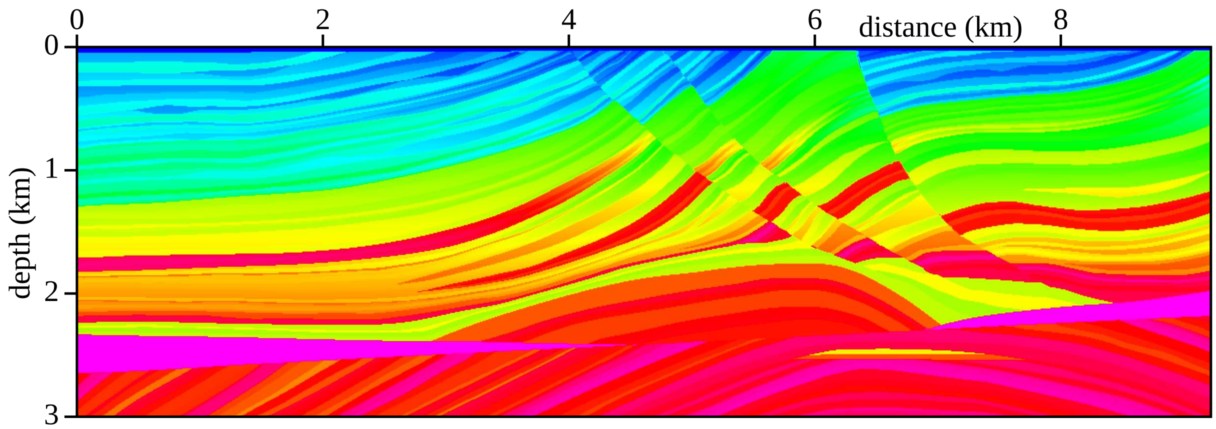

Figure 1. Marmousi model.

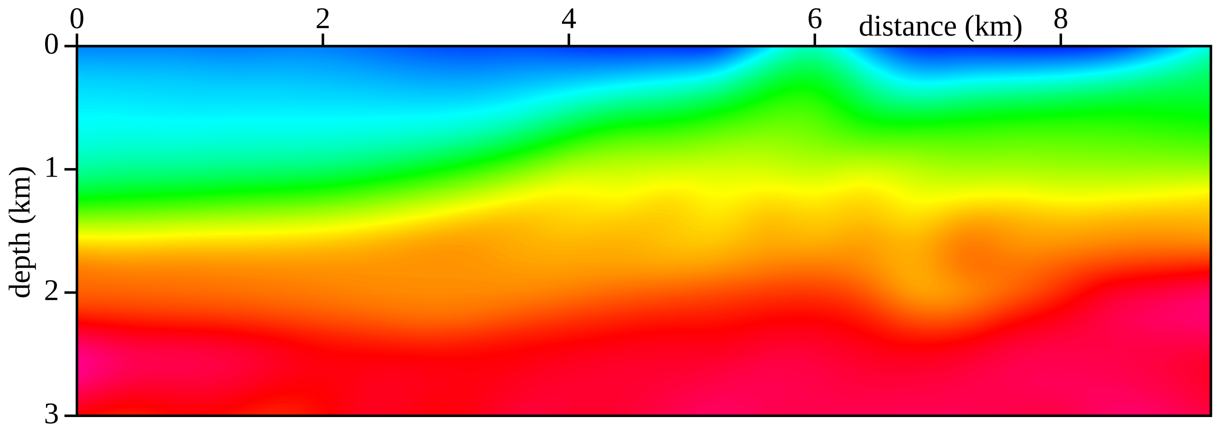

Figure 2. Smoothed Marmousi model.

3. Optimization of the shape of Gaussian packets

The envelope of optimized Gaussian packets, in the plane perpendicular to the central ray of the packet, depends not only on the frequency ω, but also on the coordinate of the intersection of the central ray of a Gaussian packet with the profile x_{R}, on its arrival time t_{R}, and on the component of the slowness vector along the profile p. Parameter $N^0(x_{\mathrm{R}}, t_{\mathrm{R}}, p)$ describes the shape of a corresponding Gaussian beam along the initial surface. Imaginary part of $\mathrm{Im}(N^0)$ determines the Gaussian beam width and real part of $\mathrm{Re}(N^0)$ defines the curvature of the wavefront. Since we are using axially symmetric Gaussian packets, and thus need to control their spreading in the plane perpendicular to the central ray of the packet, it is sufficient to optimize the initial shape of corresponding Gaussian beams (Žáček, 2005).

Žáček (2006a) presented the algorithm of the optimization of the shape of Gaussian packets for common-shot migration, but presented the numerical example of the optimization just for zero offset. Žáček (2005) did not apply the optimization in his numerical example at all.

The main improvement in comparison with the zero-offset (shot and receiver coincides) optimization presented in the numerical example by Žáček (2006a) is the possibility to compute optimized Gaussian packets for non-zero offset configurations. We used the algorithm which allows us to smooth iteratively the distribution of parameter N^0 on the Hamiltonian hypersurface. The initial shape of Gaussian packets was optimized and smoothed for each common-shot gather. In numerical calculations, we selected two different extents of smoothing of N^0. In the first calculation, the range of $\mathrm{Im}(N^0)$ (ratio of $[\mathrm{Im}(N^0)]_{\mathrm{MAX}}$ to $[\mathrm{Im}(N^0)]_{\mathrm{MIN}}$) was approximately one order of magnitude, in the second calculation, the range of $\mathrm{Im}(N^0)$ was approximately two orders of magnitude. The values of $\mathrm{Im}(N^0)$ have to be positive. For some common-shot gathers in the second calculation, the ratio had to be smaller than two orders.

It is time consuming to manually find a proper value of smoothing parameter for each common-shot gather. The values of the smoothing parameter are in a range of several orders for the whole Marmousi data set (240 shots). We smoothed the values of $\mathrm{Re}(N^0)$ with the same smoothing parameter as the values of $\mathrm{Im}(N^0)$.

The initial discretization steps Δx_{R}, Δt_{R} and Δp for optimization on the three-dimensional Hamiltonian hypersurface are equal for all shots. Figures 3, 4, 5 show examples of distribution of parameter $\mathrm{Im}(N^0)$ calculated for shot 77 (at a horizontal coordinate of 4.9 km). Figure 3 shows the optimized values, Figure 4 shows the optimized values smoothed into the range of approximately one order of magnitude and Figure 5 shows the optimized values smoothed into the range of approximately two orders of magnitude.

For the smoothed and optimized values of $\mathrm{Im}(N^0)$ and $\mathrm{Re}(N^0)$ new discretization steps Δx_{R}, Δt_{R} and Δp are calculated. These new discretization steps usually differ for individual common-shot gathers. It is necessary to recompute smoothed optimized parameters $\mathrm{Im}(N^0)$ and $\mathrm{Re}(N^0)$ on the new grid and then continue with the decomposition of the recorded wave field.

Whereas Žáček (2006a) smoothed the optimized values of N^0, we switched to smoothing the optimized values of $1/N^0$. Unlike Žáček (2006a), we carefully adjusted different smoothing in the directions of coordinates x_{R}, t_{R} and p along the Hamiltonian hypersurface.

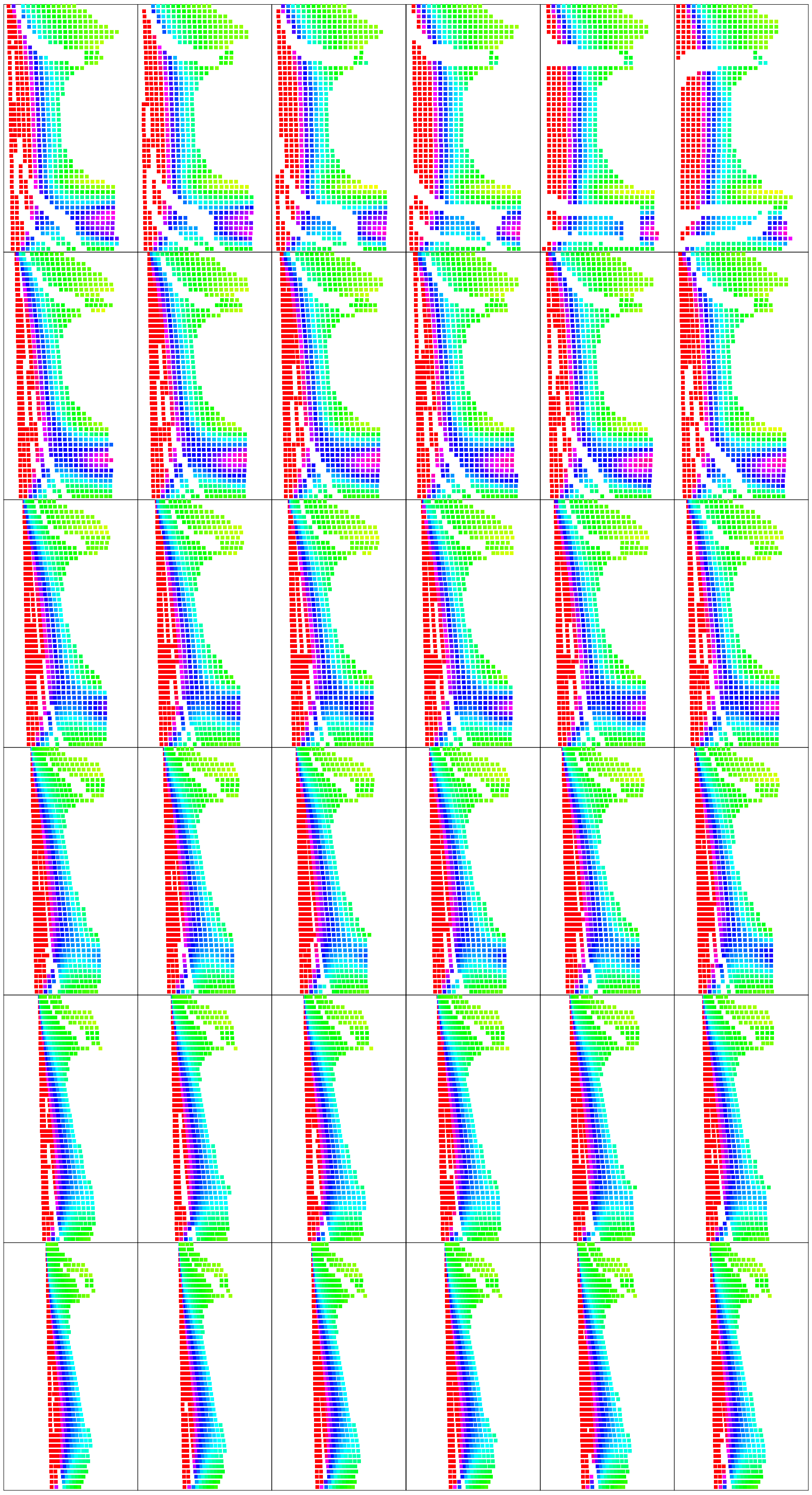

Figure 3. Distribution of the optimized initial parameter $\mathrm{Im}(N^0(x_\mathrm{R}, t_\mathrm{R}, p))$ on the Hamiltonian hypersurface for shot 77 (at a horizontal coordinate of 4.9 km). Left bottom distribution corresponds to the first and right top distribution to the last of 36 discrete values of x_R. Left bottom corner of each distribution corresponds to the minimum values of t_R and p. t_R increases horizontally and p increases vertically for each of 36 distributions. Colour scale: yellow corresponds to $\mathrm{Im}(N^0) = 0.19 \times 10^{-8}\ \mathrm{s\,m^{-2}}$, green corresponds to $\mathrm{Im}(N^0) = 0.1 \times 10^{-6}\ \mathrm{s\,m^{-2}}$, red corresponds to $0.5 \times 10^{-6}\ \mathrm{s\,m^{-2}} \leq \mathrm{Im}(N^0) \leq 3.4 \times 10^{-6}\ \mathrm{s\,m^{-2}}$.

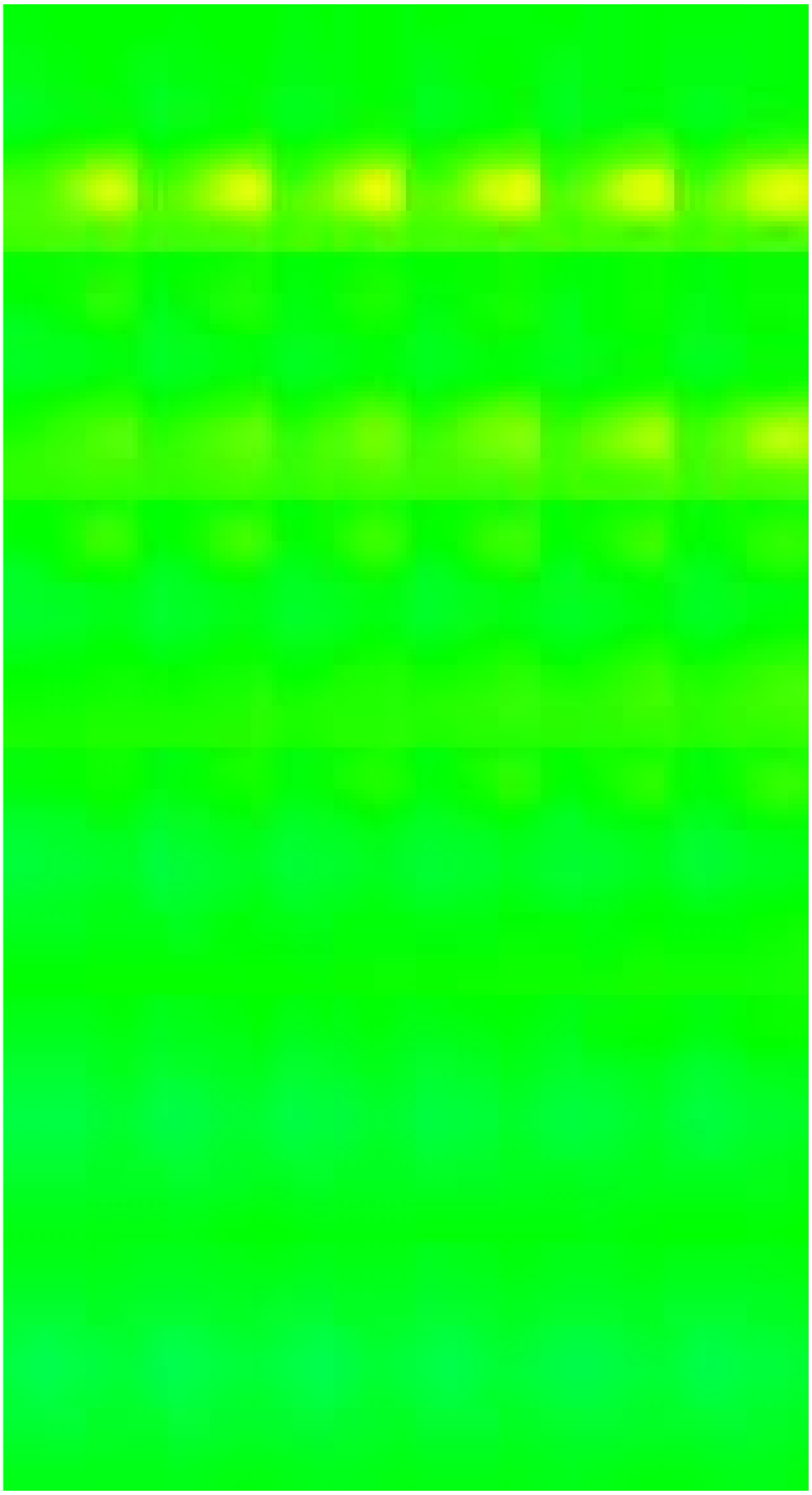

Figure 4. Distribution of the optimized and smoothed initial parameter $\mathrm{Im}(N^0(x_\mathrm{R}, t_\mathrm{R}, p))$ on the Hamiltonian hypersurface for shot 77 (at a horizontal coordinate of 4.9 km). The smoothed values varies in *one* order of magnitude. Left bottom distribution corresponds to the first and right top distribution to the last of 36 discrete values of x_R. Left bottom corner of each distribution corresponds to the minimum values of t_R and p. t_R increases horizontally and p increases vertically for each of 36 distributions. Colour scale: yellow corresponds to $\mathrm{Im}(N^0) = 0.19 \times 10^{-8}\ \mathrm{s\,m^{-2}}$ and green corresponds to $\mathrm{Im}(N^0) = 0.1 \times 10^{-6}\ \mathrm{s\,m^{-2}}$.

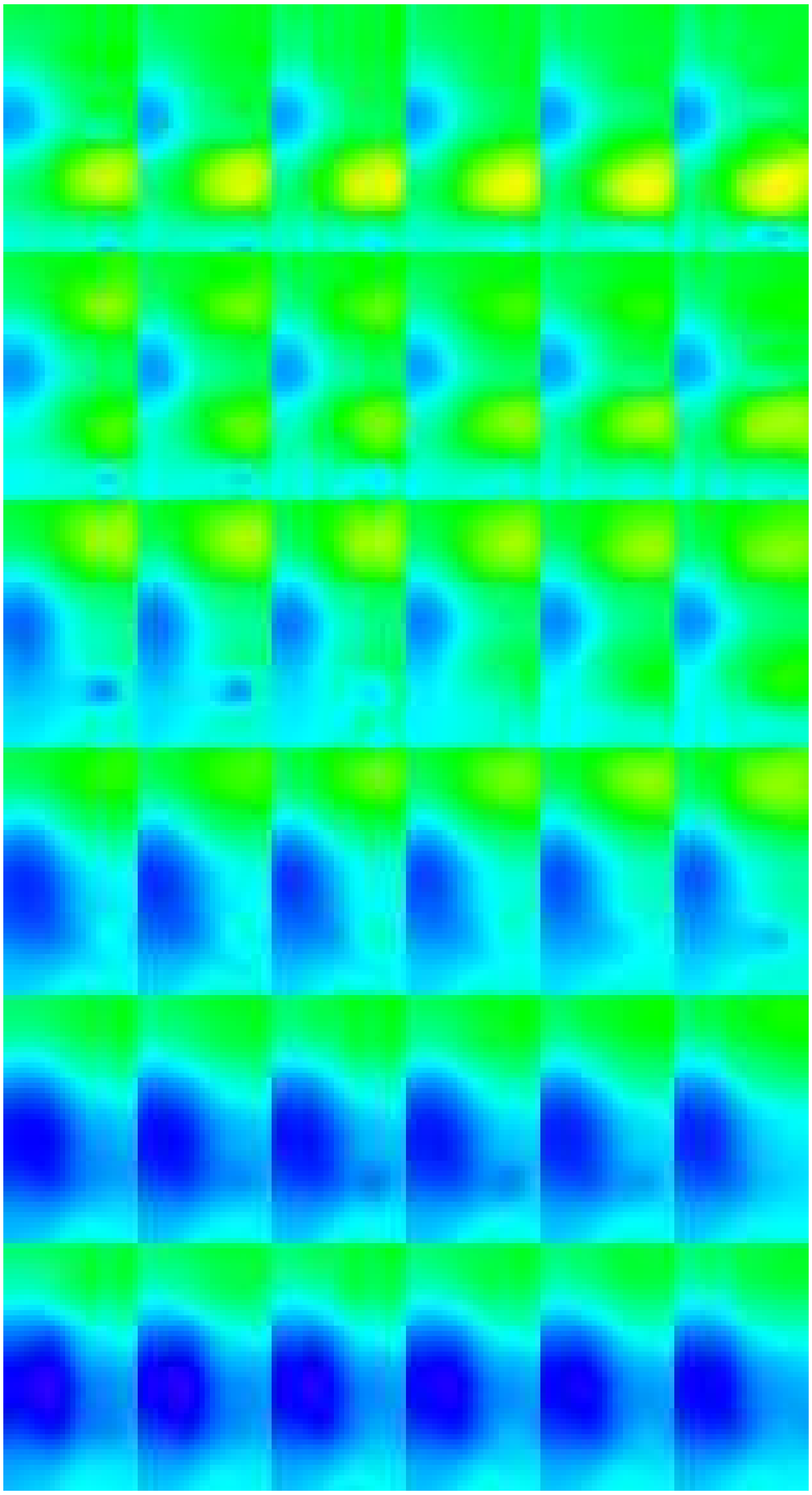

Figure 5. Distribution of the optimized and smoothed initial parameter $\mathrm{Im}(N^0(x_\mathrm{R}, t_\mathrm{R}, p))$ on the Hamiltonian hypersurface for shot 77 (at a horizontal coordinate of 4.9 km). The smoothed values vary in *two* orders of magnitude. Left bottom distribution corresponds to the first and right top distribution to the last of 36 discrete values of x_R. Left bottom corner of each distribution corresponds to the minimum values of t_R and p. t_R increases horizontally and p increases vertically for each of 36 distributions. Colour scale: yellow corresponds to $\mathrm{Im}(N^0) = 0.19 \times 10^{-8}\ \mathrm{s\,m^{-2}}$, green corresponds to $\mathrm{Im}(N^0) = 0.1 \times 10^{-6}\ \mathrm{s\,m^{-2}}$, and blue corresponds to $\mathrm{Im}(N^0) = 0.3 \times 10^{-6}\ \mathrm{s\,m^{-2}}$.

Compared to Žáček's (2005) calculation, we decreased the maximum value of horizontal component p of the slowness vector so that it does not exceed the maximum slowness in the velocity model. Žáček (2005) missed many Gaussian packets because of too great maximum value of p. On the other hand, our maximum value of p removes the Gaussian packets propagating along shallow rays from the decomposition of the recorded wave field and from the migration, which is clearly seen in Figure 6b.

4. Decomposition of the recorded wave field into optimized Gaussian packets

A serious problem of the decomposition of the recorded wave field into Gaussian packets is the computational cost (Žáček, 2006b). Žáček (2005) performed migration with uniform Gaussian packets (N^0 constant). For optimized (non-uniform) Gaussian packets, the computational cost is several times greater. In 2-D, for the imaginary part of N^0 varying from $[\mathrm{Im}(N^0)]_{\mathrm{MIN}}$ to $[\mathrm{Im}(N^0)]_{\mathrm{MAX}}$, the number of grid points in 4-D phase-space (x_{R}, t_{R}, p, ω) is approximately proportional to $\{[\mathrm{Im}(N^0)]_{\mathrm{MAX}}/[\mathrm{Im}(N^0)]_{\mathrm{MIN}}\}^{1/2}$ (Žáček, 2005). We thus sped up the computer code for the decomposition approximately twenty times in order to be able to work with optimized Gaussian packets.

One of the criteria of usability of smoothed optimized Gaussian packets is the result of decomposition of the Marmousi data set recorded wave field for each shot. The differences between the decomposed original wave field and composed approximated wave field should not be significant. Figure 6 shows example of wave-field differences for a shot 77 (at a horizontal coordinate of 4.9 km) for two different distributions of smoothed optimized Gaussian packets described in the Section 3. The wave-field differences seems to be acceptable for both results of decomposition. The greatest differences are for waves near the surface. This is probably caused by the selected maximum value of the horizontal component of the slowness vector, which removes the Gaussian packets propagating along shallow rays from the decomposition of the recorded wave field.

5. Migration

Figure 7 displays the results of the migration. Stacked migrated sections correspond to uniform and smoothly optimized (non-uniform) Gaussian packets. Two different extents of smoothing of N^0 were used. In the first case (Figure 7b), the range of $\mathrm{Im}(N^0)$ (ratio of $[\mathrm{Im}(N^0)]_{\mathrm{MAX}}$ to $[\mathrm{Im}(N^0)]_{\mathrm{MIN}}$) was approximately one order of magnitude, in the second case (Figure 7c), the range of $\mathrm{Im}(N^0)$ was approximately two orders of magnitude. The differences between the three plotted stacked migrated sections are small.

We added for comparison the stacked migrated section calculated using the Kirchhoff migration (see Figure 8). The efficiency of this method is much better than of the Gaussian packet migration. The time of the Kirchhoff migration, computed on a grid of cells 16×16 metres and interpolated to grid of cells 4×4 metres, is approximately 100 minutes. The Gaussian packet migration was computed on a grid of cells 20×20 metres and interpolated to grid of cells 4×4 metres. The time of the Gaussian packet migration with uniform packets is approximately 5 days, the time of the Gaussian packet migration with optimized packets with $\mathrm{Im}(N^0)$ differing by one order of magnitude is approximately 1 month, the time of the Gaussian packet migration with optimized packets with $\mathrm{Im}(N^0)$ differing by two orders of magnitude is approximately 4 months. The times of the computation correspond to an Athlon one core 2.0 GHz processor.

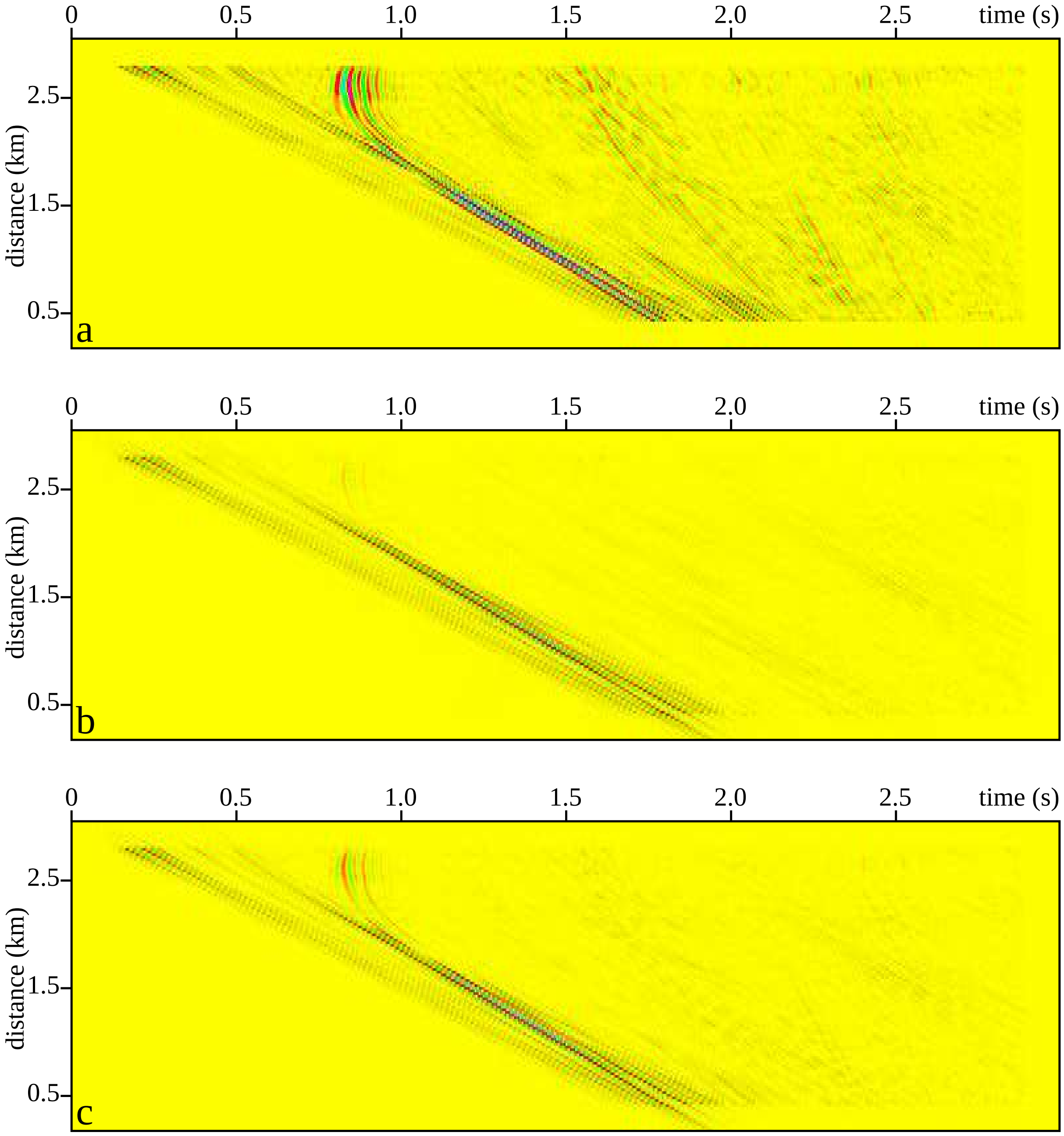

Figure 6. **Example of wave-field differences for shot 77 (at a horizontal coordinate of 4.9 km): (a) Marmousi original common-shot gather, (b) differences between original common-shot gather and approximated common-shot gather for optimized Gaussian packets with** $\mathrm{Im}(N^0)$ **differing by** *one* **order of magnitude, (c) differences between original common-shot gather and approximated common-shot gather for optimized Gaussian packets with** $\mathrm{Im}(N^0)$ **differing by** *two* **orders of magnitude. Colour scale is identical for all figures: from yellow that corresponds to zero, up to red that corresponds to the maximum amplitude.**

Software used for computations (Fortran 77 source codes, data files, history files, descriptions) is included on the SW3D-CD-12 (Bucha & Bulant, 2008).

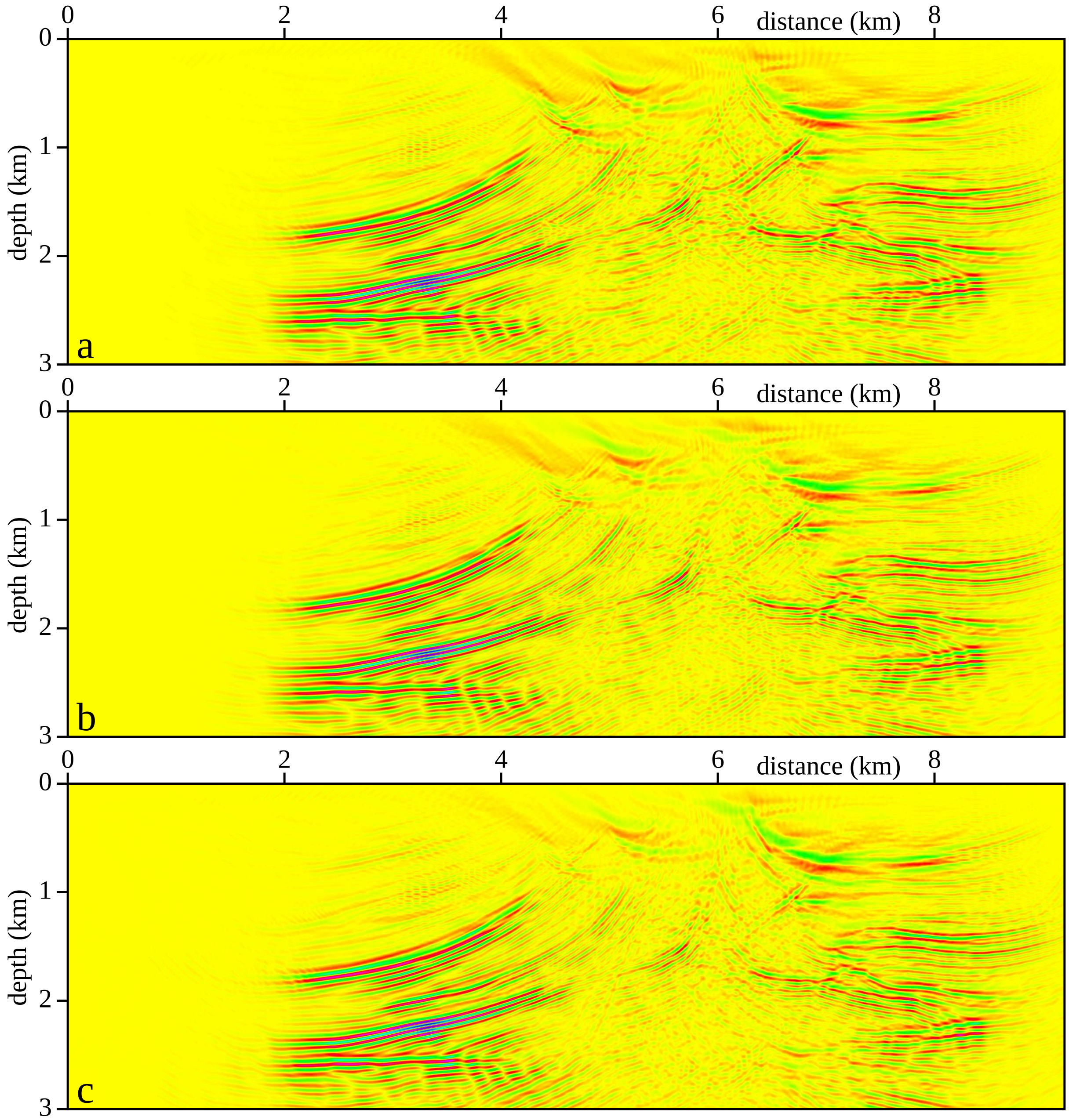

Figure 7. **Stacked migrated sections of the Marmousi data set calculated in the smoothed velocity model: (a) using uniform Gaussian packets, (b) using optimized and smoothed Gaussian packets with $\mathrm{Im}(N^0)$ differing by *one* order of magnitude, (c) using optimized and smoothed Gaussian packets with $\mathrm{Im}(N^0)$ differing by *two* orders of magnitude. We used the sparse grid of cells 20×20 metres for migration, and applied interpolation to the grid of cells 4×4 metres but no other post-processing. Colour scale differs for each figure: from yellow which corresponds to zero, up to red which corresponds to the maximum amplitude different for each figure.**

6. Conclusions

We applied the smoothly optimized (non-uniform) Gaussian packets to the Gaussian packet prestack depth migration. Although we expected improvement in the reconstruction of the bottom part of the Marmousi model, the stacked migrated sections are nearly equal for uniform and optimized Gaussian packets. Note that Žáček (2005) mentioned two other possible causes of bad reconstruction of the bottom part of the model:

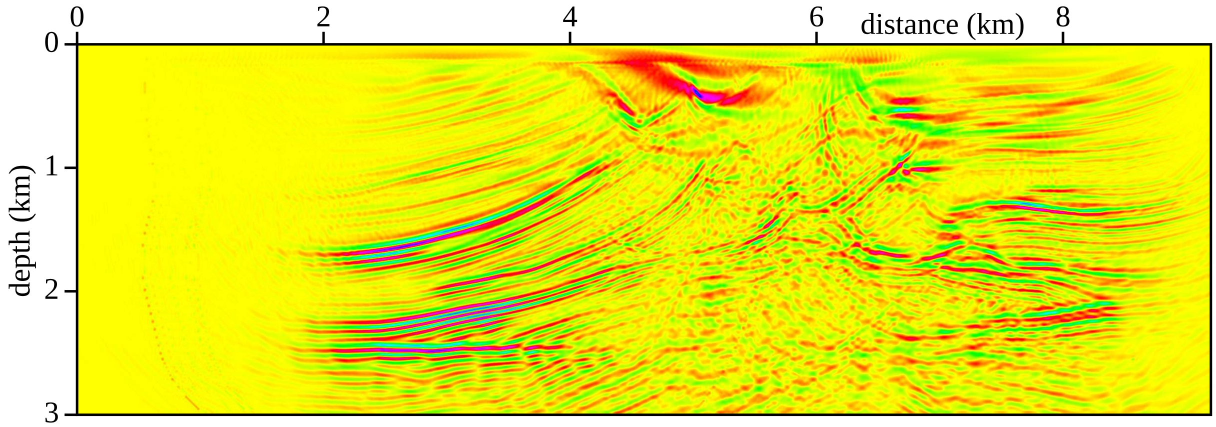

Figure 8. Stacked migrated section calculated using Kirchhoff migration. We used the sparse grid of cells 16×16 metres for migration, and applied interpolation to the grid of cells 4×4 metres but no other post-processing.

– oversimplified stacking procedure,
– considerably smoothed velocity models.

We shall perform other tests to check the accuracy and efficiency of the method.

Acknowledgments

The author thanks Luděk Klimeš for valuable comments and recommendations concerning this paper, and for his assistance in speeding up Karel Žáček's code for the decomposition of the wave field into Gaussian packets.

The research has been supported by the Grant Agency of the Czech Republic under contract 205/07/0032, by the Ministry of Education of the Czech Republic within research project MSM0021620860, and by the members of the consortium "Seismic Waves in Complex 3-D Structures" (see "http://sw3d.cz").

References

Bucha, V. & Bulant, P. (eds.) (2008): SW3D-CD-12 (DVD-ROM). In: Seismic Waves in Complex 3-D Structures, Report 18, pp. 245, Dep. Geophys., Charles Univ., Prague, online at "http://sw3d.cz".

Klimeš, L. (2000): Smoothing the Marmousi model for Gaussian-packet migrations. In: Seismic Waves in Complex 3-D Structures, Report 10, pp. 63–74, Dep. Geophys., Charles Univ., Prague, online at "http://sw3d.cz".

Versteeg, R. J. & Grau, G. (eds.) (1991): The Marmousi experience. Proc. EAGE workshop on Practical Aspects of Seismic Data Inversion (Copenhagen, 1990), Eur. Assoc. Explor. Geophysicists, Zeist.

Žáček, K. (2002): Smoothing the Marmousi model. Pure and Appl. Geophys., **159**, 1507–1526.

Žáček, K. (2005): Gaussian packet prestack depth migration. In: Seismic Waves in Complex 3-D Structures, Report 15, pp. 29–48, Dep. Geophys., Charles Univ., Prague, online at "http://sw3d.cz".

Žáček, K. (2006a): Optimization of the shape of Gaussian beams. Stud. geophys. geod., **50**, 349–366.

Žáček, K. (2006b): Decomposition of the wave field into optimized Gaussian packets. Stud. geophys. geod., **50**, 367–380.